Research Article

BIOMEDICAL Journal of Scientific & Technical Research

ISSN: 2574 -1241

DOI: 10.26717/BJSTR.2022.46.007383

Image Quality Optimization and Radiation Dose Minimization in Bone X-Ray Radiography

RL Njinga*, VM Tshivhase, RB Nshimirimana, TP Keetile and TC Dlamini

Department of Radiation Science, South African Nuclear Energy Corporation, Centre for Applied Radiation Science and Technology, North-West University, Department of Physics, University of medical sciences, Ondo City, Ondo-State, Nigeria

***Corresponding author:** RL Njinga, Department of Radiation Science, South African Nuclear Energy Corporation Centre for Applied Radiation Science and Technology, North-West University Department of Physics, University of medical sciences, Ondo City, Ondo-State, Nigeria

ARTICLE INFO

Received: September 27, 2022

Published: October 14, 2022

Citation: RL Njinga, VM Tshivhase, RB Nshimirimana, TP Keetile and TC Dlamini. Image Quality Optimization and Radiation Dose Minimization in Bone X-Ray Radiography. Biomed J Sci & Tech Res 46(4)-2022. BJSTR. MS.ID.007383.

ABSTRACT

Through the development of correlations between the X-ray scanning parameters, image quality (IQ), and radiation dose, bone X-ray radiography has been optimized. The IQ and radiation dose absorption (RDA) are maximized when the X-ray tube parameters (voltage, current, and exposure period) and sample-detector distance (SDD) are raised. For the purpose of maximizing bone X-ray radiography, the optimal trade-off between maximum IQ and minimal RDA was discovered, and the associated X-ray scanning settings were chosen. The study of the effects of X-ray tube voltage, X-ray current, X-ray exposure time, and SDD resulted in the formulation of the X-ray scanning parameters. Both the IQ and the radiation dose deposition rise as all X-ray tube settings are increased. For the purpose of maximizing X-ray radiography through decreasing the radiation dosage, the X-ray scanning parameters, such as the X-ray tube voltage of 100 kV, X-ray tube current of 100 A, X-ray exposure time of 1 sec, and the SDD of 80 cm, were obtained. With these settings, the RDA was less than 1.00 mSv and the permissible diagnostic reference dose, radiation dose standards were met using this radiation dose.

Keywords: Bone X-Ray Radiography; Sample-Detector Distance; Image Quality; Radiation Dose Absorption; X-Ray Exposure Time

Introduction

The X-ray radiation is defined as electromagnetic radiation capable of passing through the object and reveals the interior structure of that object in the form of an image. This type of radiation was discovered by the German scientist Wilhelm Rontgen Carl A [1]. X-ray radiation is extensively used in medical and industrial applications primarily due to its ability to penetrate dense materials such as bones and reveal their actual anatomy Umadevi [2]. The X-ray radiation is transmitted through the patient during medical diagnosis. X-ray radiography is one of the common imaging techniques that employ X-ray radiation to reveal the internal structures of the objects. Abnormalities or diseases such as tooth decay, lung cancer, cervical cancer, kidney stones, blood clots and cardiac diseases are usually diagnosed through X-ray examinations such as dental X-ray, pelvis X-ray, chest X-ray and abdominal X-ray examinations (RSNA, 2010). The importance of acquiring high quality images in medical imaging is a necessity to enable ultimate accurate diagnosis. The X-ray radiation is characterized as ionizing radiation due to its ability to ionize atoms. Ionizing radiation is generally hazardous to the human body Desouky, et al. [3].

The X-ray photons passing through the human body undergo absorption inside the cell tissues. Subsequently, the ionization of biological molecules takes place. The alteration of molecules inside the body occurs and accordingly causes damage to the cells Ullman [4]. The concept of optimization in X-ray radiography examinations is the process of finding the best compromise between the quality of the radiograph and RDA for the particular X-ray examination Nyathi [5]. The objective of optimization in X-ray radiography is to enhance the desired benefits of this imaging technique without compromising the well-being of the patients. The strategies of optimization are often implemented in X-ray radiography as a tool to ensure that negligible radiation exposures are maintained during examinations. The reduction of radiation exposures to patients in X-ray examinations is a difficult process because the purpose of examination itself is often the deciding factor between the amounts of radiation exposure required to produce a certain level of IQ Uffmann [6]. Optimization is necessary for reduction of radiation doses and ensuring that sufficient information is attained at an ideal quality of the image in a certain X-ray examination for a specified medical or industrial purpose.

Ideally, it is meaningless to use X-ray radiography to obtain the image of a certain defective bone if the surrounding soft tissues will receive high levels of radiation dose Hendee [7,8]. To achieve optimization of IQ, optimum balance between X-ray tube voltages, X-ray tube current, exposure time and source detector distance should be study in correlation with harmful effects inflicted into the patient's body during the X-ray examination. This study explores the optimization of the quality of the image obtained from a bone X-ray radiography procedure with minimized radiation dose deposition in the surrounding soft tissue. The effect of X-ray scanning parameters will be established and thereafter optimization will be explored. The establishment of the X-ray scanning parameters that will yield the best quality image at minimized radiation dose will be studied. In addition, the X-ray scanning parameters, and the insightful knowledge of the use of phantoms and real samples to explore means of optimizing the X-ray radiographs and the associated RDA will be examined.

Materials and Methods

The Micro-focus X-ray machine used in this study is based at South African Nuclear Energy Corporation (Necsa) radiation science unit. The machine is an imaging modality that allows the acquisition of the interior information of an object non-destructively and non-invasively Hoffman [9]. The main components of this system are X-ray tube, a sample holder/stage and 2D high system resolution flat panel detector encapsulated within the lead-lined cabinet Hoffman [9]. The function of the lead-lined cabinet is to maintain the radiation dose below 1 micro-Sievert per hour Hoffman [9]. The power rating of Micro-focus X-ray machine is approximately 30 W which allows the scanning of quite a variety of samples with different densities. The system consists of a voltage range of 30 kV-225 kV and a beam current of 0-1 mA. The focal spot on the anode metal target ranges up to 0.003 mm. The flat panel detector installed in the Micro-focus X-ray machine consists of a 16-bit dynamic range of up to 65335-pixel value. The X-ray experiments in which the acquisition of radiographs of phantoms and real samples was done by varying each X-ray scanning parameter while others were kept constant.

The same X-ray scanning settings used to acquire the radiographs of phantoms and real samples were used to measure the RDA with radiation dose detector (Identifinder Ultra of physical dimension 25 cm×9 cm×8 cm and weight of 1250g). The background radiation was measured before the experiment ICX Technologies [10]. The measurements of radiation dose were achieved by placing the Identifinder Ultra detector on the sample stage of the X-ray machine and the X-ray scanning parameter of interest were varied exactly the same way as it was varied during the acquisition of radiographs. The actual samples used were body parts of a rat obtained at Wits University, South Africa. The samples were the rat humeri (arm bone), femora (thigh bone), tibias (shinbone) and skulls (complete rat head). The samples were stored in 10 % buffered formalin solution in plastic containers for preservation purpose. The use of musk as a precautionary measure to reduce inhalation of the formalin solution in areas with poor ventilation was adhered to throughout the study. The width of each rat bone was measured using the Vernier Calliper. The samples were gathered together before the experiment and each sample was dried using a paper towel prior to scanning.

The defined thickness of acrylic glass was used to replace the soft tissue of the rat limb bones. The thickness of acrylic glass was tailored according to the thickness of the actual rat tissue. Three phantoms of different thicknesses were designed using aluminium metal and acrylic glass. The different thicknesses of aluminium metal and acrylic glass were representing the average of different thicknesses of rat limb bones, human palm bones and human limb bones. The aluminium block was embedded inside the acrylic glass. The phantoms representing the thicknesses of the human limbs and palm were designed in accordance with Huang, et al., (2012); Singh, et al. (2014); Osborne, et al. [11]; Garrido Varas & Thompson (2011); Pan, (1924); Higgins, (1895); Alexander & Viktor, (2010) and Cuk, et al. (2012). The average of the three thicknesses of the compact bone of the human limbs and soft tissues were calculated. This thickness was used to tailor the thickness of aluminium metal and acrylic glass to design the phantom representing the thickness of the human limbs. The thicknesses of the soft tissues and compact bone of the human palm were obtained from Singh, et al. (2014); Osborne, et al. [11]; Garrido Varas & Thompson, (2011);

Pan, (1924); Higgins, (1895) and Alexander & Viktor, (2010) to design the phantom.

Each thickness of the real tissues was multiplied by 2 (X-ray beams will transverse the phantom twice during transmission). Each sample was dried before the scan. The samples and phantoms were supported using polystyrene foam material during the scan as illustrated in (Figure 1). The mass attenuation coefficient of the polystyrene foam material causes negligible X-ray attenuation. Hence, this material was adopted for support and stabilization of the sample during the scan. (Figure 1) shows the polystyrene foam material supporting the samples or phantoms which were positioned properly on the stage inside the Micro-focus X-ray machine during the scan. The stage was tilted prior to scanning using the external control panel of the Micro-focus X-ray machine for optimal spatial resolution. This adjustment ensures that the sample is fully visualized in the 2D radiograph's field of view. The Identifinder Ultra detector was positioned along with the samples and phantoms on the stage in relation to the X-ray source at the specified SDD during the measurements as shown in (Figure 1). The X-ray scanning parameters that were used to acquire the radiographs of rat samples and phantoms were also used to measure the radiation dose Thermo Fisher Scientific [12].

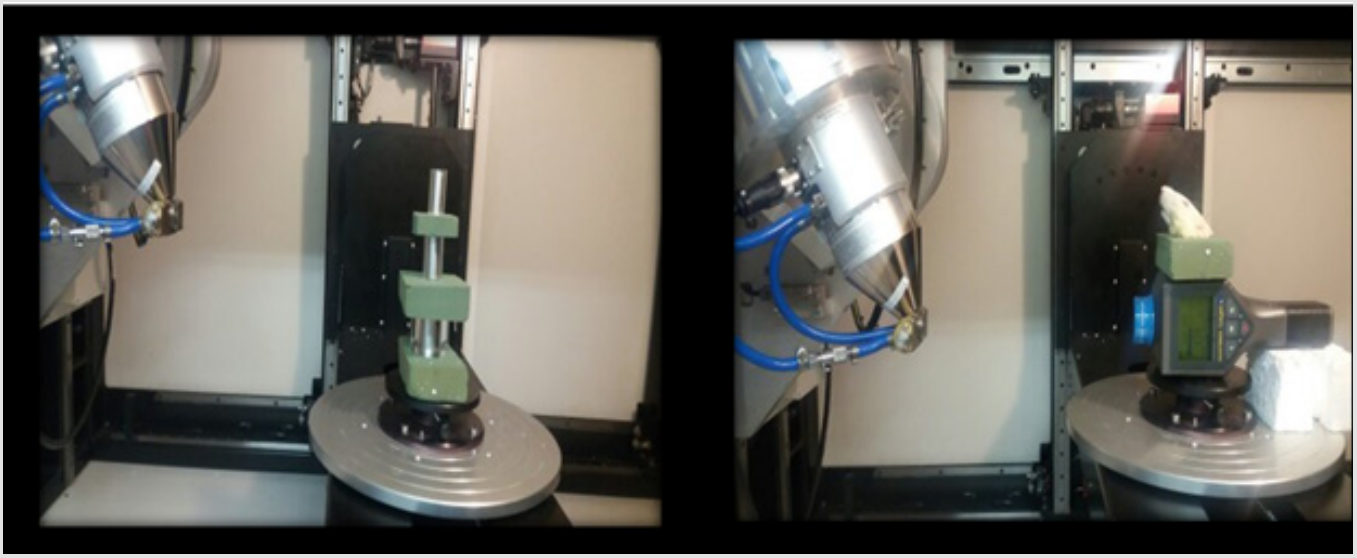

Figure 1: Positioning of the sample and phantoms on the stage.

Results and Discussion

As revealed in (Figure 2), the IQ of the phantoms simulating the human limbs, rat limbs and the real samples of the rat tibia, femur, and humeri, increased with an increase in the X-ray tube voltage from 30 kV to 175 kV. No image was formed within the X-ray tube voltage range of 30 kV – 50 kV during the imaging of the skull. Also, no images of the human palm phantom were formed within the range of 30kV to 40kV. The IQ was not evaluated for X-ray tube voltages that did not produce any images. Low X-ray tube voltages produce low energy X-ray photons, and these photons are completely attenuated by some of the thickness of the samples and phantoms. Hence, there was no image formation during the scan of some of the rat samples and human palm phantom. According to the observations made in (Figure 2), the phantoms and the rat samples responded similarly to the X-ray exposure, as there was a linear increase in IQ throughout the increase in X-ray tube voltage. Although no radiation dose was absorbed from 30kV – 60kV, radiation dose increased as the X-ray tube voltage was increased from 60 kV to 175 kV as shown in (Figure 3). This similar trend between the samples and phantoms is due to the small difference in the material composition and thicknesses.

However, throughout the increase in RDA, rat samples absorbed more radiation dose than phantoms. The IQ was maximized as the RDA for both phantoms and rat samples increased as seen in (Figure 4). The maximum quality images of the phantoms were acquired with low RDA, whereas the acquisition of the high-quality images of the rat samples were acquired with high RDA. The difference in the maximization of IQ in relation to radiation dose between the phantoms and the samples is due to the density of the actual tissues (bones and soft tissues) and materials that were used to simulate them (aluminium and acrylic glass). The density of aluminium ($0.0027 g/cm^3$) that was used to simulate bones in phantoms was less than the density of the dominant mineral (Calcium ~1.54 g/cm3) found in actual bones of the samples used in this

study (Figure 3). The RDA of the rat samples and the phantoms versus X-ray tube voltage investigation the optimal quality images in (Figure 4). were formed at RDA above 20.28 µSv, this radiation dose corresponds to the X-ray tube voltage of 90 kV and above as shown in (Figure 3). The optimal quality images were acquired with the X-ray tube voltage above 100 kV in (Figure 2), the corresponding radiation dose at 100 kV in (Figure 3) is 29.99 µSv.

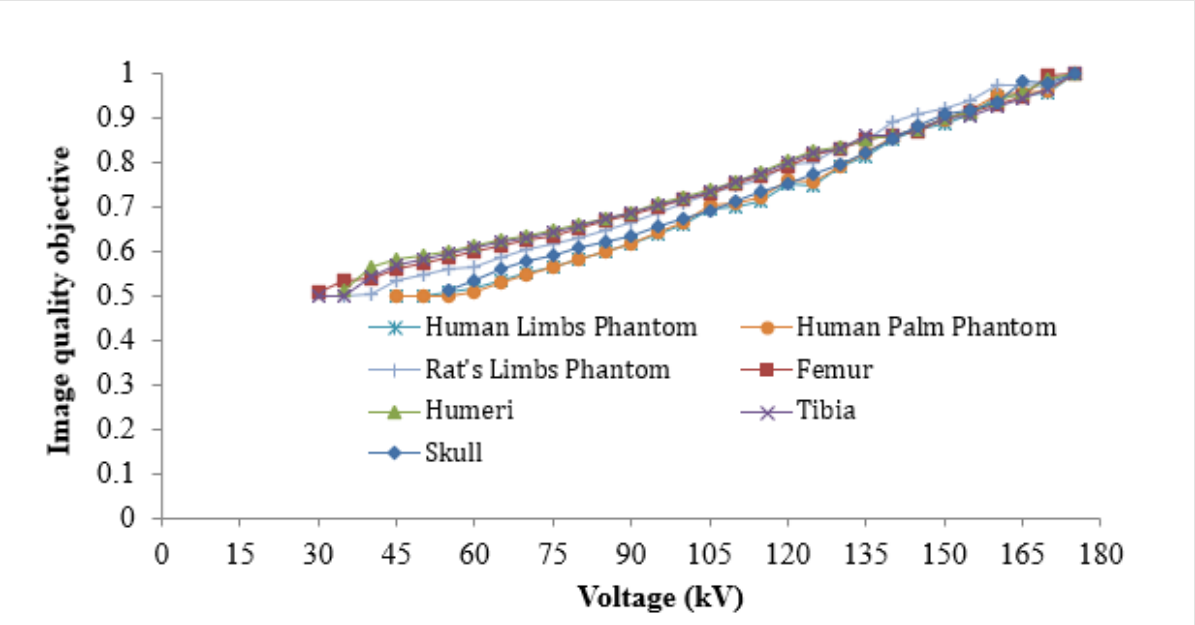

Figure 2: The effect of X-ray tube voltage on IQ.

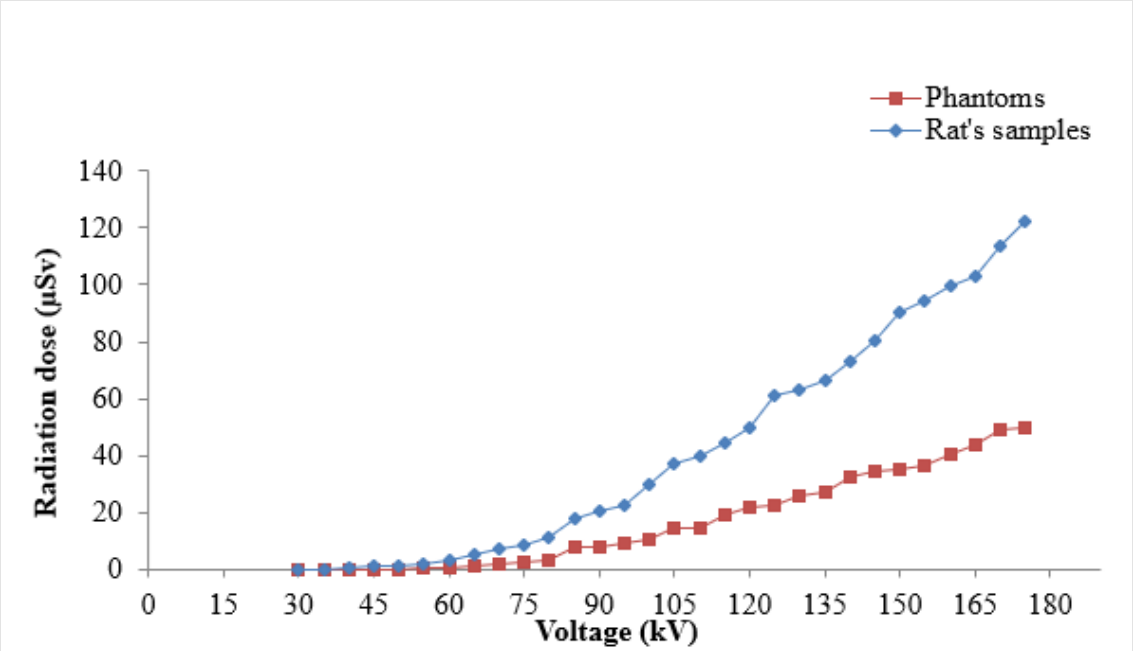

Figure 3: The RDA of the rat samples and the phantoms versus X-ray tube voltage investigation.

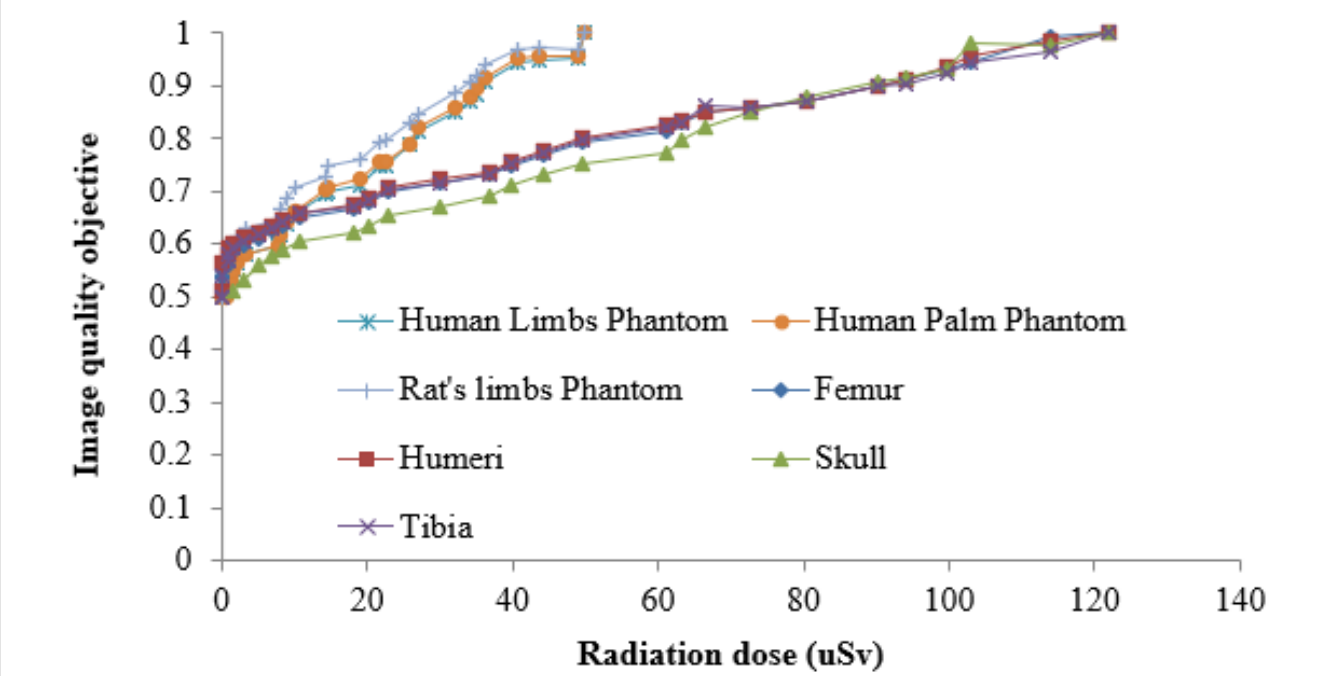

Figure 4: IQ of the radiographs of the rat samples and phantoms versus radiation dose for X-ray tube voltage investigation.

This radiation dose is within the limit of radiation reference level that was stipulated by Dianna D. Cody, 2018, in which the radiation reference level less than 100 μSv was suggested when acquiring the radiographs of the hand, wrist and the finger. In this regard, the findings of this study suggest that the X-ray tube voltage of 100 kV with X-ray tube current of 100 μA, X-ray exposure time of 1 sec and maximum SDD of 80 cm can be safely used for optimization of bone images in X-ray radiography. (Figure 5) shows that the acquisition of the radiographs of the rat samples and phantoms were done by varying the X-ray tube current from 5 μA-190 μA. During the investigation of the X-ray tube current, the X-ray tube voltage was constant at 100 kV, X-ray exposure time at 1 second, SDD at 50 cm. There was a small dissimilarity between the maximization of the IQ of the actual samples and phantoms throughout the increase in X-ray tube current from 5 μA-190 μA as seen in (Figure 5). The relationship between IQ and X-ray tube current is linear. However, few points are observed to be deviating from the linear trend at X-ray tube current values between 5 μA-20 μA. Although there was an insignificant difference in IQ between the rat samples and phantoms, the RDA between the phantoms and rat samples was considerably different as seen in (Figure 6).

The phantoms used in this study absorbed low radiation dose than the rat samples as the X-ray tube current was increased from 5 μA-190 μA. The RDA was very minimal below the X-ray tube current of100 μA, this region constitutes low quality images, whereas the region above the X-ray tube current of 100 μA produced high quality images. The specific relationships were observed independently between IQ and radiation dose as the X-ray tube current was increased as seen in (Figures 5&6). This phenomenon implies that the thicknesses of the bone and soft tissue simulating materials were responding similarly to the actual tissues of the samples under the X-ray exposure when X-ray tube current was varied. Unlike the rat samples, high quality images of the phantoms were acquired with low radiation absorption in (Figure 7). The difference in the atomic numbers is responsible for the variation in IQ and RDA between the phantoms and samples in (Figure 7). The rat samples consist of bones and bone tissues are made up of calcium with atomic number 20, aluminium metal with atomic number 13, was simulating the bone tissue in the phantoms. The high atomic number molecules absorb more X-ray radiation than low atomic number molecules Dendy, et al. [13].

Hence, (Figure 7). shows that the samples absorbed more radiation dose than phantoms in this study. The findings of this study do not correspond with the findings of Olubamiji [14], who concluded that no significant change in IQ can be achieved through variation of X-ray tube current. In this study, the quality of radiographs was successfully increased by increasing the X-ray tube current between 5 μA and 190 μA with the X-ray tube voltage of 100 kV, X-ray tube exposure time of 1 second, SDD of 80 cm and no X-ray filtration. The optimum quality radiographs were obtained with the X-ray tube current of more than 100 μA. The implication there of is that when high X-ray tube voltage (such as 100 kV) is considered when ac-

quiring optimized radiographs of the bones, the corresponding selection of low X-ray tube current (lower than 100 µA) values should also be considered. However, the findings of this study shows that high quality images are acquired with the X-ray tube current of above 100 µA; the constraint thereof is the RDA. 3000 µSv-5000 µSv is a designated diagnostic reference when acquiring radiographs of the human skull Vano, et al. [15]. The optimal radiographs of the rat bones and phantoms obtained in this study occurred at an absorbed radiation dose less than the diagnostic reference dose at 12 µSv and 59 µSv with the X-ray tube current of 100 µA [16-25].

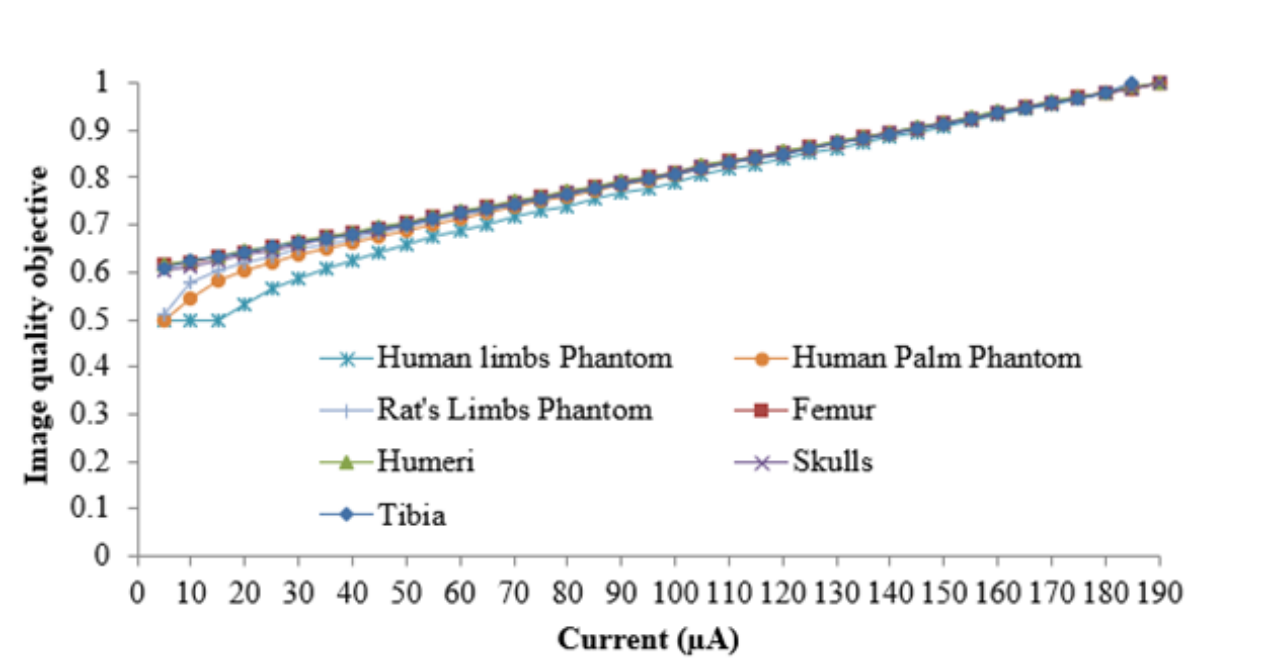

Figure 5: The IQ of the radiographs of the rat samples and phantoms as the X-ray tube current is varied.

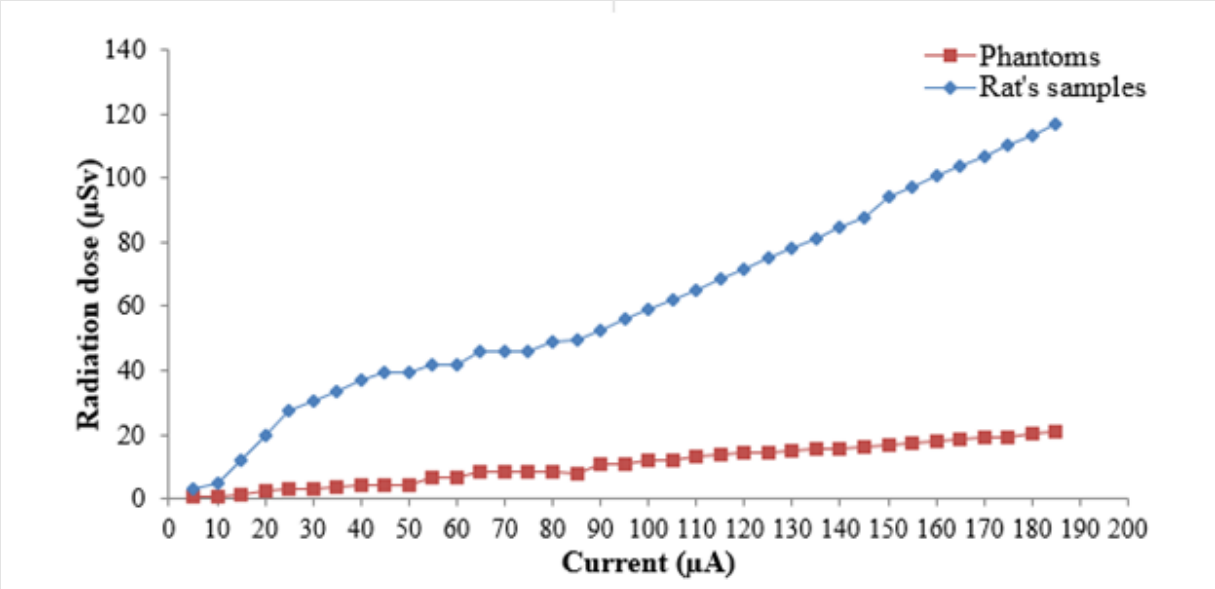

Figure 6: The RDA of the rat samples and phantoms versus X-ray tube current investigation.

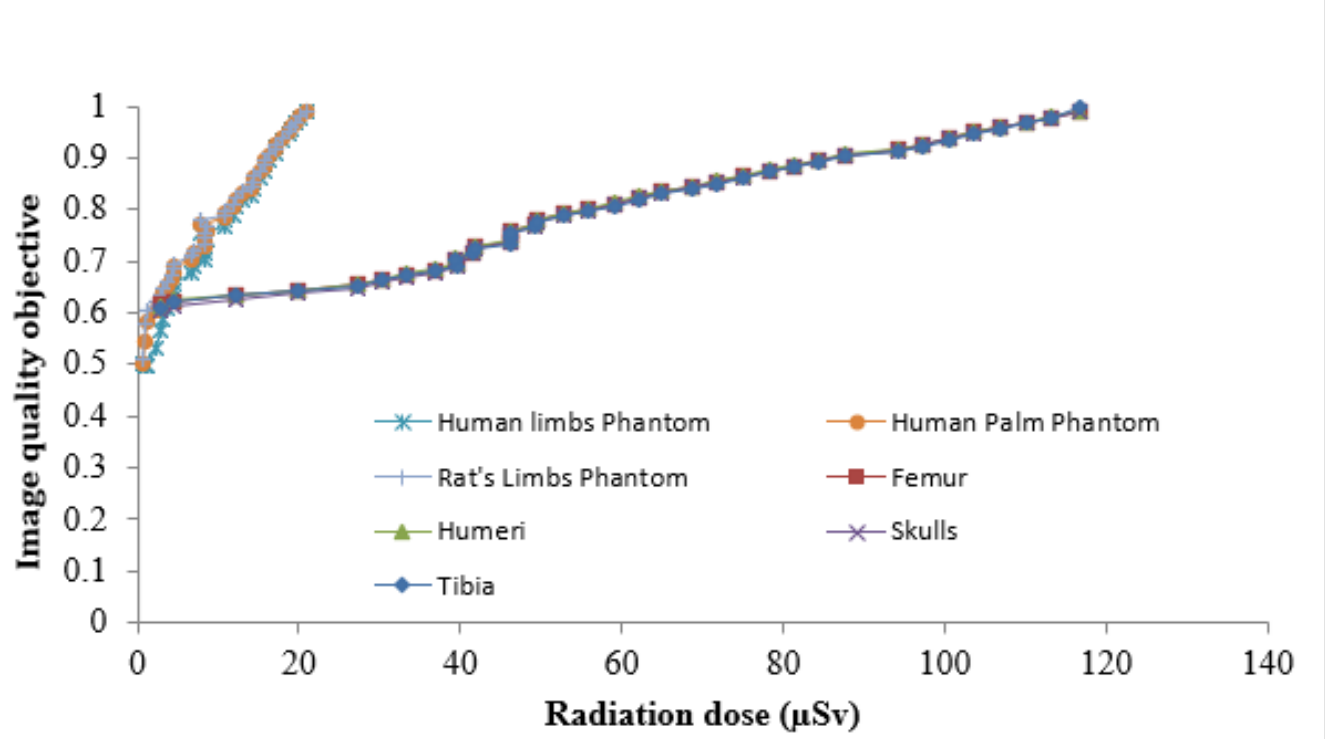

Figure 7: The IQ of the radiographs of rat samples and phantoms versus RDA for X-ray tube current investigation.

Therefore, this X-ray current with the X-ray tube voltage of 100kV can be used for optimization in X-ray radiography without harming the well-being of the patient. The quality of the images of both the rat samples and phantoms was increasing when the X-ray tube exposure time was increased from 0.267 second to 4.000 seconds. A linear relationship between the IQ, RDA and X-ray tube exposure time as presented in (Figure 8& 9). The increase in X-ray exposure time in (Figure 8) increases the IQ for both the samples and phantoms. Although the phantoms absorbed less radiation dose than real samples, a linear relationship between radiation dose and exposure time was observed in (Figure 9). The RDA of both phantoms and samples increased with different slopes at 30.08 & 7.64. High quality images of the phantoms were acquired with low radiation dose as shown in (Figure 10). The optimal images in (Figure 10). were acquired between the RDA of 8.00 µSv to 132.00 µSv. This RDA correspond to X-ray exposure time between 1 second to 4 seconds as seen in (Figures 8&9) shows that the images that were obtained at the X-ray exposure time of 4 seconds are more optimal for both phantoms and samples [26-33].

The radiation dose of 31.00 µSv and 132.00 µSv were absorbed by the phantoms and rat samples respectively when the optimal quality images were acquired at the X-ray exposure time of 4 seconds. The radiation reference level of 100 µSv for X-ray examinations of the hand, thumb, knee and the wrist. According to these studies, the acquisition of optimized bone radiographs was achieved at an X-ray exposure time of 4 second, X-ray voltage and current of 100 kV and 100 µA and SDD of 80 cm. The IQ of all the rat samples and phantoms had a slight increase throughout the increase in SDD, meaning the quality of all the images was almost constant as the samples and phantoms were approaching the X-ray source as seen in (Figure 11). Although a slight increase in IQ was observed when the SDD was increased from 42 cm to 100cm, all the images of phantoms had much higher quality than all the images of the rat samples. Although the images of the rat skull had the least IQ throughout the investigation, all the images of the rat samples had the same maximum quality at the SDD of 100 cm. The phantom representing the human limbs had the least IQ when compared to other phantoms from 42 cm to 95 cm [34-48].

At 100 cm, the quality of the images of this phantom increased to maximum quality images. However, the quality of the images of the phantoms simulating the thickness of the human hand (palm) and rat limbs were the same throughout the increase in SDD from 42 cm to 100 cm. As seen in (Figure 12), the real samples absorbed more radiation dose than the phantoms. The radiation dose increased throughout the increase in SDD with respect to the IQ. Although the images were optimal at the SDD between 40 cm to 100 cm as seen in (Figure 11), the RDA rapidly increased for both phantoms and actual rat samples (Figure 12). At the SDD of 80 cm

and 100 cm, the obtained RDA for the rat samples were 58.61 µSv & 113.61 µSv and the phantoms were 31.11 µSv & 73.06 µSv respectively. As shown in (Figure 13), there is a trend between the RDA and the related IQ of the rat samples and the phantoms. Apart from the thickness of the phantoms, other dimensions of the phantoms were bigger than that of the actual rat samples. This brings about the discrepancies as seen in the plot (Figure 13). The height of acrylic glass and aluminium of phantoms were 6 cm and 3 cm whereas the average height of the rat tibia, femur and humeri was 2.5 cm [49-58].

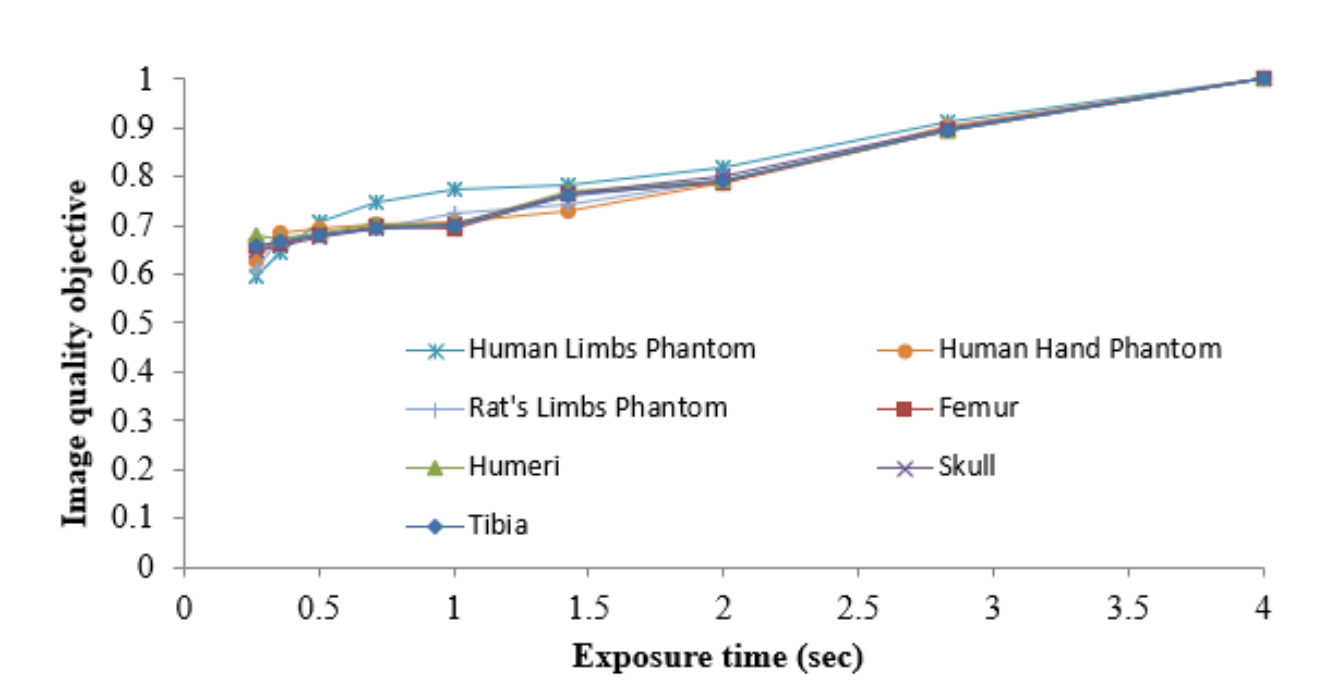

Figure 8: The IQ of the radiograph's variation with X-ray tube exposure time.

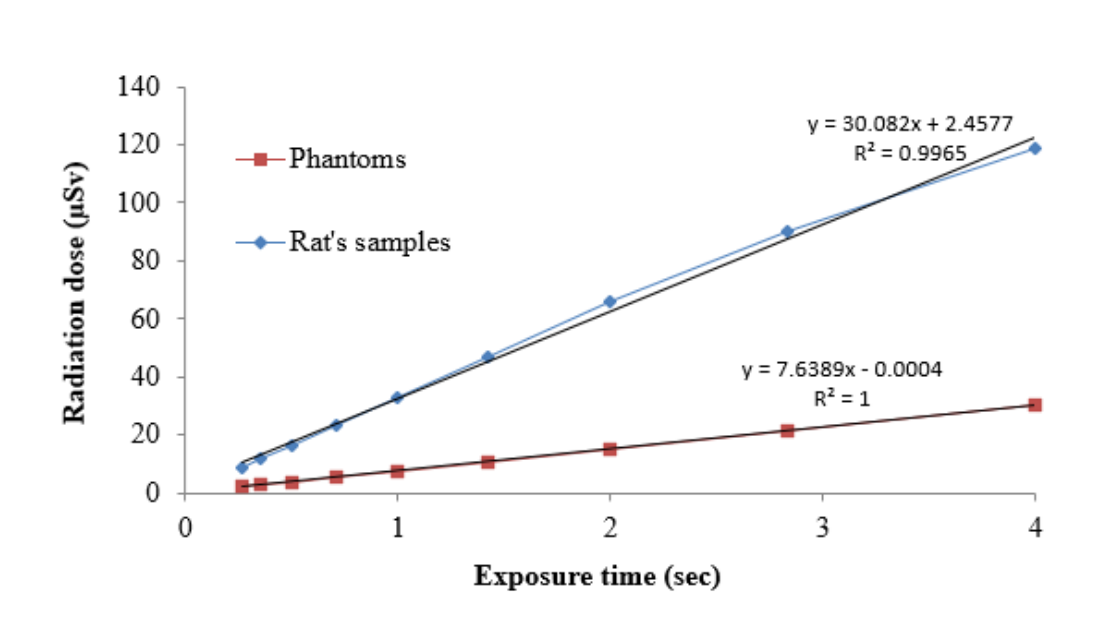

Figure 9: The RDA variation with X-ray tube exposure time.

DOI: 10.26717/BJSTR.2022.46.007383

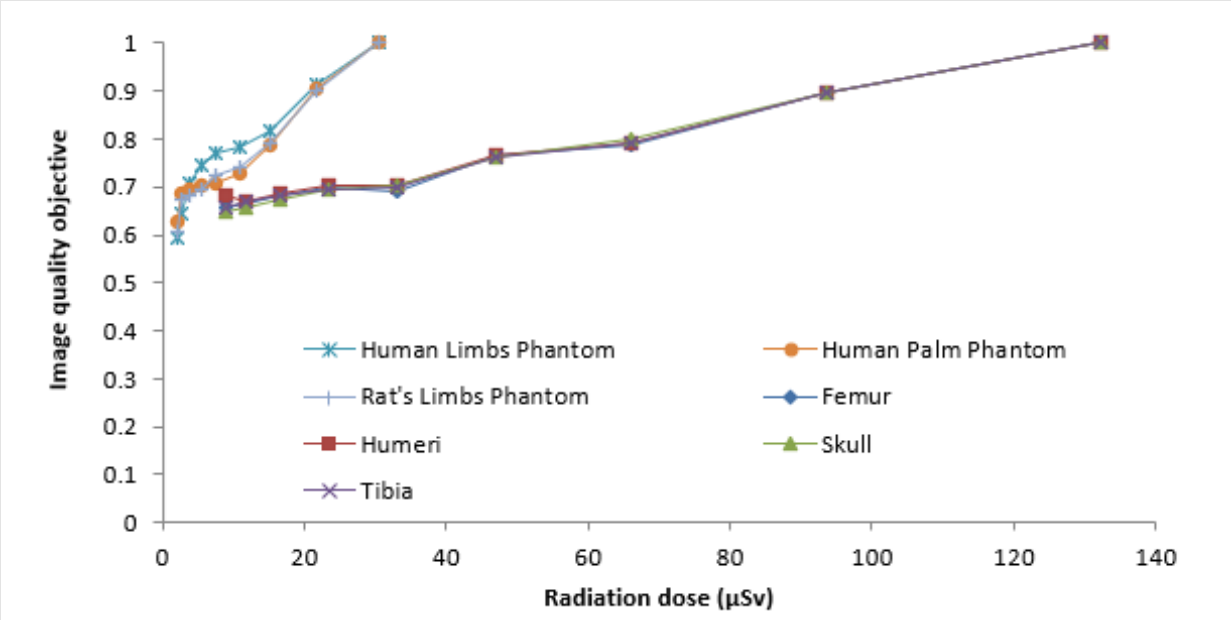

Figure 10: the effect of IQ and RDA for X-ray tube exposure time investigation.

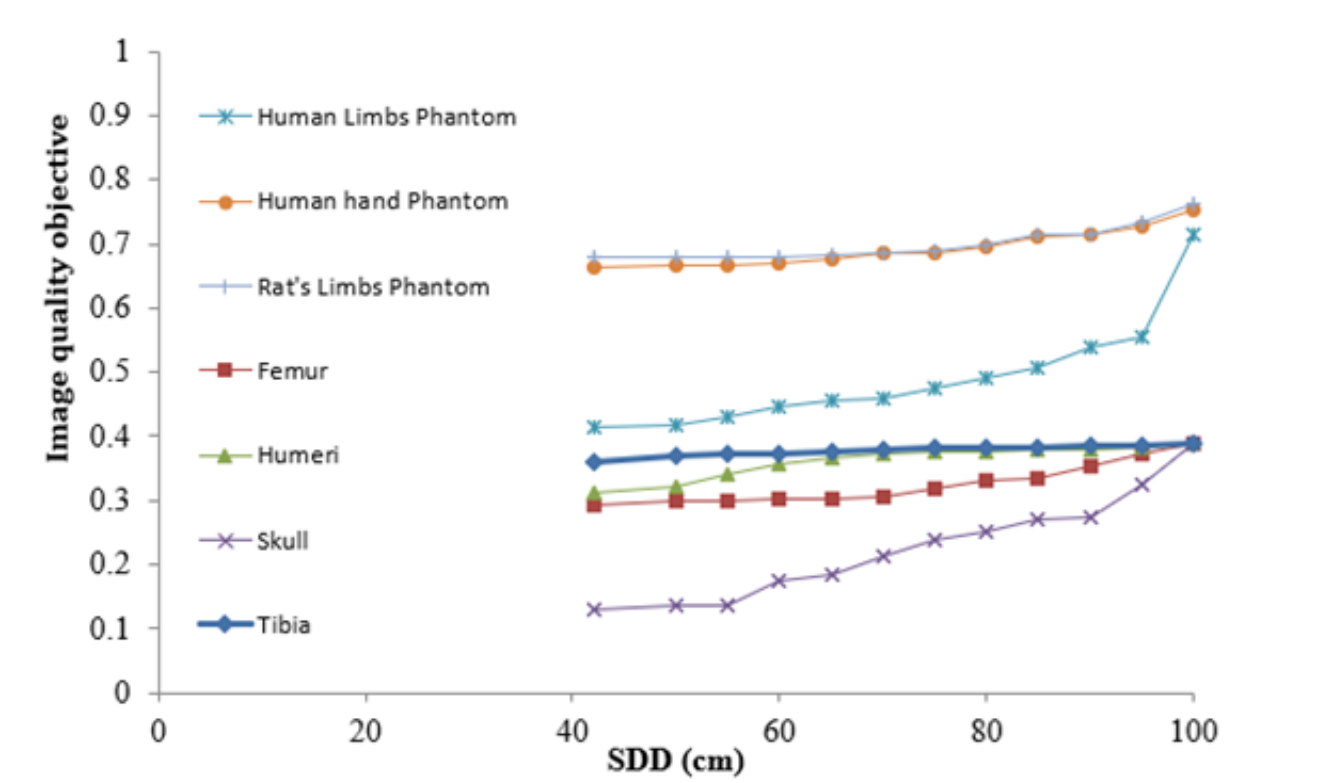

Figure 11: The effect of the IQ and SDD investigation.

DOI: 10.26717/BJSTR.2022.46.007383

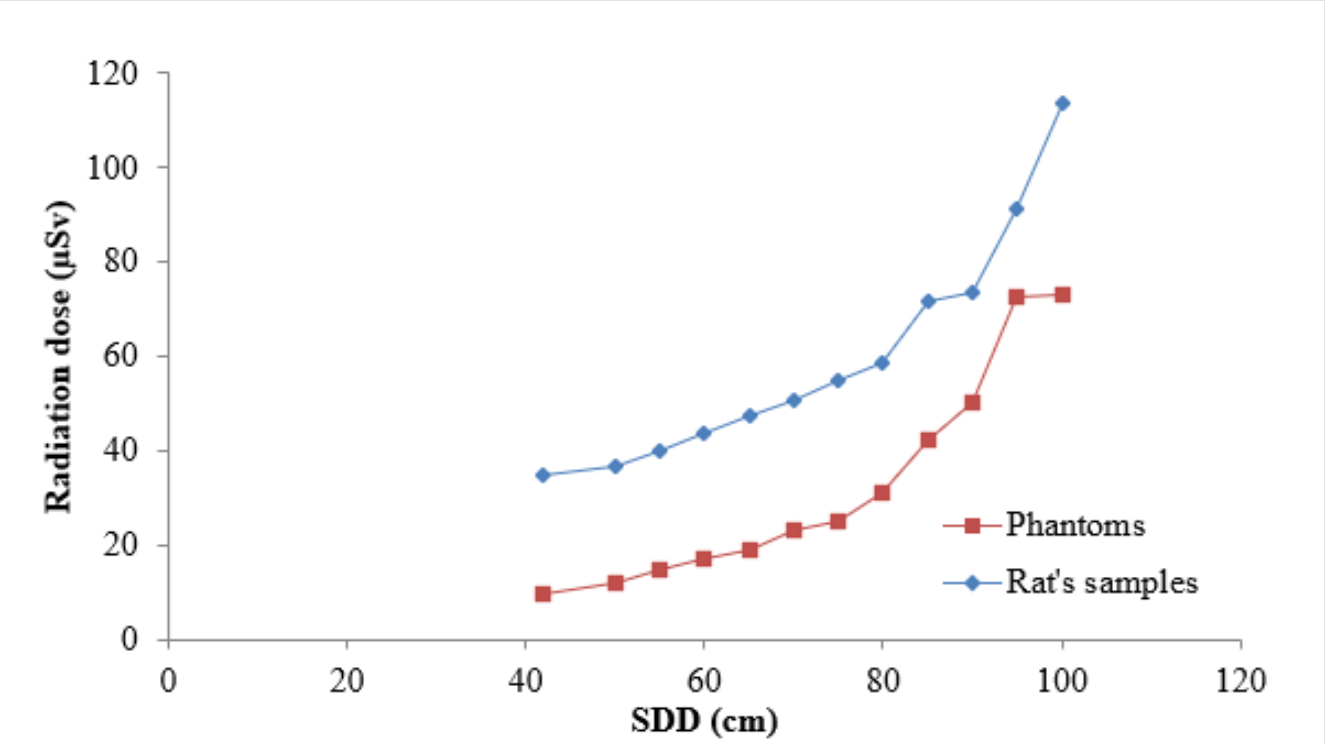

Figure 12: The effect of RDA and SDD.

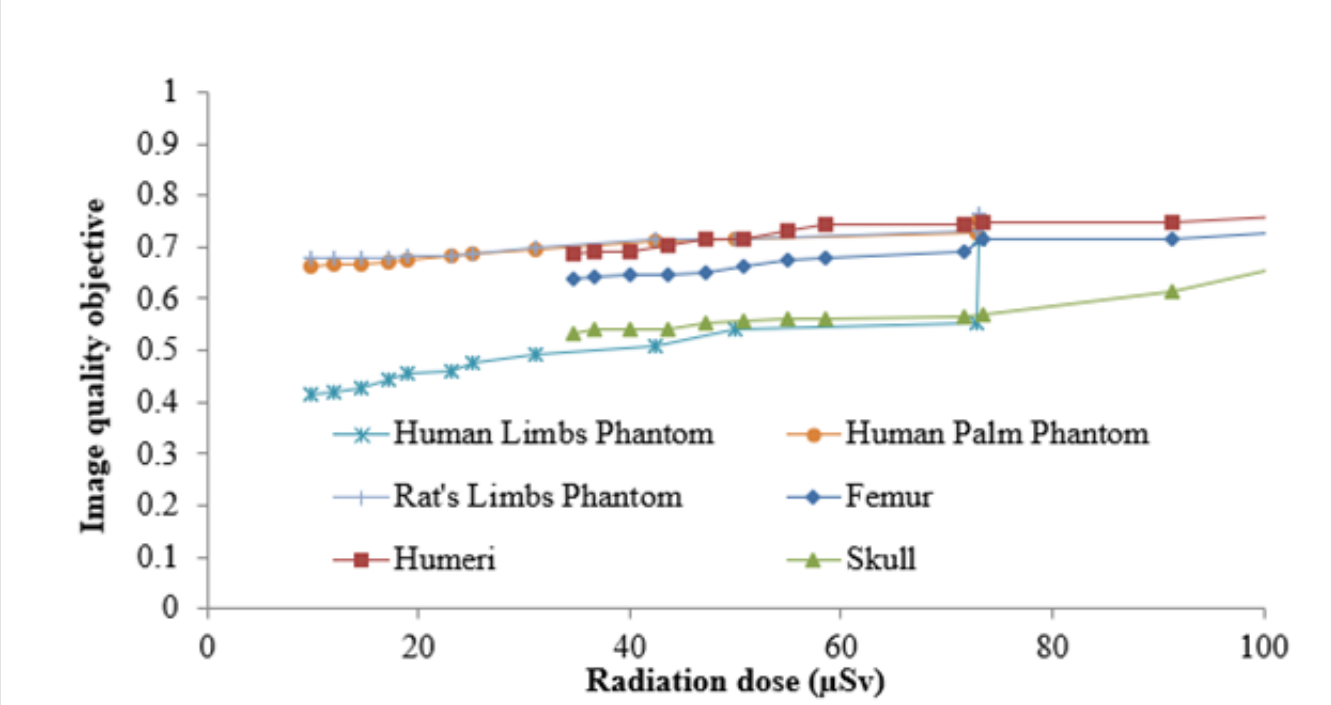

Figure 13: The IQ variation with respect to RDA.

The specification stated by Busch et al. 2004 indicate that in conventional X-ray radiography, the images of the shoulders, upper arm and lower leg should be obtained with the distance of 100 cm to 150 cm between the film and the focus (commonly known as FFD). According to Busch et al. 2004 the X-ray tube voltage should be within the range of 60 kV to 75 kV and the X-ray exposure time less than 100 milliseconds. As study by Dianna, 2018 indicate that the radiation reference level of less than 100 µSv should be specified by for X-ray examinations of the human limbs. In this studies, the optimal quality images of the rat samples and the phantoms were obtained with RDA of 58.61 µSv and 113.61 µSv for SDD of 80 cm and 100 cm. At the SDD of 100 cm, the obtained RDA was slightly greater than 100 µSv and at the SDD of 80 cm, the obtained RDA was below the reference limit with a value of 58.61 µSv [59-67].

Conclusion

The optimization of bone X-ray radiography was achieved through the establishment of the relationship between X-ray scanning parameters IQ and radiation dose. Increasing the X-ray tube parameters (voltage, current and exposure time) and SDD maximized the IQ and the RDA. The best compromise between maximum IQ and minimized RDA was found and the corresponding X-ray scanning parameters were selected for optimization of bone X-ray radiography. The selected X-ray scanning parameters were established through the investigations of the effect of X-ray tube voltage, X-ray current, X-ray exposure time and sample detector instance. The increase in all the X-ray tube parameters increases both the IQ and the radiation dose deposition. The slight increase in IQ can be achieved by the increase in the SDD while considering the rapid accumulation in radiation dose deposition. The X-ray scanning parameters such as the X-ray tube voltage of 100 kV, X-ray tube current of 100 µA, X-ray exposure time of 1 sec and the SDD of 80 cm were selected for optimization of X-ray radiography through reduction of radiation dose.

References

1. Carl AC, Gudrun Alm C (1996) Basic physics of X-ray imaging, Sweden: Faculty of Health Sciences Linköping University pp. 9-29.
2. Umadevi N, Geethalakshmi S (2011) A brief study on human bone anatomy and bone. IJCES International Journal of Computer Engineering Science pp. 93-104.
3. Desouky O, Ding N, Zhou G (2015) Targeted and non-targeted effects of ionizing. Journal of Radiation Research and Applied, 8(2): 247-254.
4. Ullman G (2008) Quantifying IQ in. Linköping University Medical Dissertations 1050 pp. 1-85.
5. Nyathi T (2012) Dose Optimization in Diagnostic Radiology, Johannesburg: University of the Witwatersrand.
6. Uffmann M, Schaefer-Prokop C (2009) Digital radiography: The balance between IQ and required. European Journal of Radiology 72(2): 202-208.
7. Hendee W, Ritenour E (2002) Medical Imaging Physics. 4th (Edn.)., New York: Wiley-Liss pp. 536.
8. Hendee WR, Ritenour ER (2002) Analytical description of IQ. In: B. Hillary, ed. medical imaging physics. 4th (Edn.)., New York: Wiley-Liss Inc pp. 281-287.
9. Hoffman JW, Frikkie C De Beer (2012) Characteristics of the Micro-Focus X-ray Tomography Facility (MIXRAD) at Necsa in South Africa. Durban, South African Nuclear Energy Corporation (Necsa) pp. 1-12.
10. ICX Technologies, (2003) Unique hand-held radionuclide, Virginia.
11. Osborne DR, Shikui Yan, Alan Stuckey, Lindy Pryer, Tina Richey, et al. (2012) Characterization of X-ray Dose in Murine Animals Using microCT, a New Low-Dose Detector and nanoDot Dosimeters. Plosone 7(11): e49936.
12. (2008) Thermo Fisher Scientific. Radiation Detection & Measurement, Massachusetts.
13. Dendy P, Heaton B (1999) Physics for Diagnostic Radiology. 2nd (Edn.)., Phidelphia, PA: Institute of Physics Publishing pp. 446.
14. Olubamiji A (2011) The influence of filtration, tube current and number of projections on CBCT IQ, Finland: Medical Imaging Centre.
15. Vano E, Jose Miguel Fernandez, Jose Ignacio Ten, Eduardo Guibelalde, Luciano Gonzalez, et al. (2002) Real-time Measurement and Audit of Patient Undergoing Computed Radiography. Radiology 225(1): 283-285.
16. Abimbola J M (2013) A nonlinear weights selection in weighted sum for convex multiobjective optimization, Ile-Ife, Nigeria. Ser Math Inform 27(3): 357-372.
17. Akmal S, Zhonghµa S (2013) Radiation dose measurements in coronary CT angiography. World J Cardiol 5(12): 459-464.
18. Andiscoa D, Blancob S, Buzzia A (2014) Dosimetry in radiology. Radioprotection / Update in radiology 78(2):114-117.
19. Bacher K (2006) Evaluation of IQ and patient radiation dose in radiology, Ghent, Belgium: University of Medicine and Health Sciences Universitiet Gent.
20. Begum Z (2001) Entrance surface dose measurement for some of the radiological patients in Bangladesh. Málaga, IAEA in Austria pp. 85-193.
21. Blancob S, Andiscoa D, Buzzia AE (2014) Dosimetry in radiology Rev Argent Radiol 78(2): 114-117.
22. Bushberg JT, Anthony Seibert J, Edwin Leidhold MJ, Boone JM (2002) Radiation detection and measurements. In: R. Joyce, ed. The essential physics of medical imaging. 2nd (Edn.)., Phidelphia: Lippincott Williams & Wilkins pp. 628-668.
23. Chougule A (2005) Reference Doses in Radiological Imag 11(2): 1425-4689.
24. (2017) CIRS ATOM Dosimetry Verification Phantoms model 701-706, Norfolk: Computerized Imaging Reference Systems Inc.
25. Dance DR, Evans S H, Skinner C L, Bradley A G (2012) Diagnostic Radiology with X-Rays. In: M. A. Flower, (Eds.)., Webb's Physics of Medical Imaging. 2nd (edn.)., Boca Raton: Taylor & Francis Group: pp. 14-91.
26. David E, William EM, Winslow J (2009) Physical phantoms for experimental radiation dosimetry. In: X Xie George & E Keith F, (Eds.)., Handbook of Anatomical Models for Radiation Dosimetry. 1st (Edn.)., London: CRC Press Taylor and Francis group pp. 389-407.
27. Denis G, Pelli B (2013) Measuring contrast sensitivity. Vision Research 90(15): 10-14.
28. Dumela KE (2010) Optimizing patient protection during diagnostic

procedures - developing diagnostic reference levels at the Dr George Mukhari Hospital, Polokwane, SA: Faculty of medicine.

29. Ervin B, Podgorsak E (2005) External Photon Beams: Physical Aspects. In: Radiation Oncology Physics: A Handbook for Teachers and Students. Vienna, Australia: International Atomic Energy Agency pp. 3-162.

30. Faiz M K (2003) Measurement of absorbed dose. In: J Pine, M Standen & LR Kairis, (Eds.)., The physics of radiation therapy. 3rd (Edn.)., Minneapolis, Minnesota: Lippincott Williams & Wilkins pp.106-154.

31. Farah A (2016) Weighted Scalarization versus Compromise Solution in Multi-Objective Economic Dispatch for Microgrids, Montreal: McGill University.

32. Garret N (2007) Multidiscpline Design and Optimization, Colorado Springs, CO: John Wiley & Sons, Ltd.

33. Garrett WR, Splettstosser HR, Titus DE (1980) Radiography in Morden Industry. Rochester, New York: Eastman Kodak Company.

34. Gupta A K, Veena C, Niranjan K (2013) Diagnostic Radiology: Recent Advances and Applied Physics in Imaging. 2nd (Ed.)., New Delhi: Jaypee Brother Medical Publishers.

35. Harbison S, Martin A (2006) An Introduction to Radiation Protection, London: Hodder.

36. Hess R, Neitzel U (2012) Optimizing IQ and dose for digital radiography of distal pediatric extremities using the contrast-to-noise ratio. Fortschr Röntgenstr 184(2012): 643-649.

37. Hirotaka N (2005) Multi-objective optimization and its engineering applications, Konan: Konan University.

38. (2007) ICRP The 2007 Recommendations of the International Commission of Radiological Protection. Annals of ICRP Publication 103(12): 1-35.

39. Institute of Physics and Engineering in Medicine, 2002. A good practice guide on all aspects of inonizing radiation protection in the clinical environment, NewYork, UK: IPEM Publications Committee.

40. (2001) International Commission on Radiological Protection 93. Managing patient dose in digital radiology, Netherlands: Elsevier.

41. Jakob W, Blume C (2014) Pareto Optimization or Cascaded Weighted Sum: A Comparison of Concepts 7(1): 166-185.

42. Kristopher S (2013) Learn ImageJ, Los Angeles: Bryan W. Jones.

43. Ladia A, SG Skiadopoulos, CP Kalogeropoulou, PE Zampakis, GG Dimitriou, et al. (2016) Radiation Dose and IQ Evaluation in Paediatric Radiography. International Journal of New Technology and Research (IJNTR) 2(3): 9-14.

44. Leea SC, Wanga J, Liuc SC, Jiang SH (2007) Evaluation of dose–image-quality optimization in digital chest radiography. Nuclear Instruments and Methods in Physics Research 580(1): 544-547.

45. Martin C, (2002) Interactions of ionising radiations with matter. In: D Sutton, (Eds.)., Practical Radiation Protection in Health Care. Oxford, UK: Oxford University Press pp. 8-20.

46. Mayles P, Nahum A, Rosenwald J C (2007) Handbook of radiotheraphy physics-theory and practice. Revised ed. New York: Taylor & Francis Group, LLC.

47. (2000) McGraw-Hill Concise Encyclopedia of Physics Parallel-plate ionization chamber., Columbia: The McGraw-Hill Companies, Inc.

48. Michael YM, Thomas PL, David O J (2004) Basic radiology. North Carolina, Raleigh: The McGraw-Hill.

49. Pacella D (2015) Energy-resolved X-ray detectors: The future of diagnostic imaging. Reports in Medical Imaging 8(10): 1-13.

50. Palomo J, Rao SP, Hans M (2008) Influence of CBCT exposure conditions on radiation dose. Oral Surg Oral Med Oral Pathol Oral Radiol Endod 105(6): 773-778.

51. Parkinson AR, Balling RJ, Hedengren J D (2013) Optimization methods for engineering design, Provo, Utah: Addison-Wesley Publishing Company.

52. Paulo RC (2013) Computer tomography phantom applications. In: A Larry, MK DeWerd, (Eds.)., The Phantoms of Medical and Health Physics: Devices for Research and Development. 1st (Edn.)., Madison: Springer Science & Business Media pp. 123-142.

53. (2016) Radiology Key. The X-ray Beam. General radiology 1(5): 2.

54. (2010) Roentgen-Roehre. svg: Hmilch. Coolidge side-window tube (scheme), Augsburg: Roentgen-Roehre. svg.

55. (2018) RSNA Radiationinfor. Org North America: Radiological Society of North America, Inc.

56. Ruiz F, F Ruiz, M Pérez-Martínez, J López, I Tort Ausina, et al. (2000) Patient dose from barium procedures. The British Journal of Radiology 73(871): 752-761.

57. Seakamela T (2016) A Study of Cracks using Micro-Focus X-ray Computed Tomography and Fractal Geometry. Johannesburg: Faculty of Science.

58. Shrimpton P, Wall B, Fisher E (1981) The tissue equivalence of Alderson Rando anthropomosphic phantom for X-rays of diagnostic qualities. Phys Med Biol 1(26): 9-133.

59. Sprawls P (1985) The Physical Principles of Medical Imagings. 2nd (Eds.)., Madison, Wisconsin: Medical Physics Publishing

60. Sprawls P (1994) The Physical Principles of Medical Imaging. Atlanta, GA, USA: A Wiley Company.

61. Timothy Marler R, Jasbir Arora S (2009) The weighted sum method for multi-objective optimization: new insights 41(6): 853-862.

62. Tootell A, Szczepura K, Hogg P (2014) An overview of measuring and modelling and modelling dose and risk from ionising radiation for medical exposures. Radiography 20(4): 323-332.

63. Unruh J (2015) Stowers Institute ImageJ Plugins Page, Kansas City: Stowers Institute for Medical Research.

64. Weck Od, Kim IY (2004) Adaptive Weighted Sum Method for Bi-objective Optimization, California: Massachusetts Institute of Technology 29(1): 149-158.

65. Whaites E (2002) The biological effects and risks associated with X-rays. In: Essentials of dental radiography and radiobiology. 3rd (Ed.)., London, UK: Churchill livingstone 29-32.

66. Whaites E, Cawson RA (2002) Essentials of Dental Radiography and Radiology. 3rd (Eds.)., London: Churchhill Livingstone.

67. White D R (1978) Tissue substitudes in experimenatal radiation physics. Med Phys 5(6): 467-479.

ISSN: 2574-1241

DOI: 10.26717/BJSTR.2022.46.007383

RL Njinga. Biomed J Sci & Tech Res

Submission Link: https://biomedres.us/submit-manuscript.php